THE ASTROPHYSICAL JOURNAL, 333:353–358, 1988 October 1

FRACTAL STRUCTURE OF INTERSTELLAR CIRRUS

D. BAZELL
Applied Research Corporation
AND
F. X. DÉSERT
Laboratory for Astronomy and Solar Physics, NASA/Goddard Space Flight Center
Received 1987 September 28; accepted 1988 March 22

ABSTRACT

We have investigated the fractal structure of some of the infrared cirrus discovered by *IRAS*. The clouds we studied are characterized by a perimeter with fractal dimension 1.26 ± 0.04 using the method of Lovejoy. This dimension was found to be essentially constant from region to region. We compare methods of calculating this dimension and discuss the relation of this quantity to some other observable cloud properties.

Subject headings: infrared: sources — interstellar: matter

I. INTRODUCTION

Recently there has been much interest in a class of geometrical objects known as fractals. Fractals are self-similar under a scale change from r_0 to $r < r_0$; the number of self-similar sections present at scale r is

$$N(r) = (r_0/r)^D , \quad (1)$$

where D is the fractal dimension of the object. D is in general nonintegral. From this scaling relation one can show (see Hentschel and Procaccia 1984) that if D is the fractal dimension of the perimeter of the object, then the area and perimeter are related by

$$(\text{area})^{1/2} = K \times (\text{perimeter})^{1/D} . \quad (2)$$

Clearly, if $D = 1$, as in the case of a circle or square, the usual relation holds between area and perimeter.

A plot of log perimeter versus log area will give a straight line with slope $D/2$ and an intercept $-D(\log K)$. If we were to make such a plot for circles and squares of different areas, we would find that each gives a straight line with the same slope ($\frac{1}{2}$) but different intercept ($-\log 2\pi^{1/2}$ for the circle and $-\log 4$ for the square). It is the slope that relates to the dimension of the object, whereas the intercept characterizes the object's shape. These ideas are discussed in more detail below.

The fractal dimension is a useful way of characterizing the geometry of many objects occurring in nature (Mandelbrot 1983). Lovejoy (1982) was the first to show that the perimeter of clouds and regions of rain in the Earth's atmosphere could be characterized by a fractal dimension of ~ 1.35. Subsequent measurements of hail clouds yielded a similar dimension (Rys and Waldvogel 1986). Henderson-Sellers (1986) has analyzed *Viking* images of Mars and found a fractal dimension of 1.6 for Martian clouds. These results regarding terrestrial clouds have been interpreted in terms of a simple theory of turbulent diffusion by Hentschel and Procaccia (1984).

We have applied similar techniques to images of "infrared cirrus" clouds detected by the *Infrared Astronomical Satellite* (*IRAS*) (Low *et al.* 1984). The cirrus has a wispy structure which is generally associated with 21 cm H I emission and can sometimes be associated with high-latitude molecular clouds (Weiland *et al.* 1986).

II. DATA AND REDUCTION

Our sources of data were the Sky Flux plates from the *IRAS* sky survey. Because we were interested in the brightness of the cirrus, we removed the foreground emission due to the zodiacal dust. In general the 25 μm *IRAS* band is dominated by emission from the zodiacal dust, so an appropriate scaling of the 25 μm brightness can yield a good estimate of the contribution of the zodiacal emission to the 100 μm image. To find the scaling factor, we chose a region in each 100 μm image that had minimal cirrus emission and measured the brightness of this region at 100 μm and 25 μm. We then scaled the entire 25 μm image by the 100 μm/25 μm brightness ratio to obtain an estimate of the zodiacal emission in the 100 μm band. This was subtracted from the 100 μm plate to produce our working image. For details and a comparison of methods refer to Verter (1987).

We chose three regions to study. Two, plates 29 and 65, were examined by eye and appeared to consist mainly of filamentary cirrus clouds. Both plates appear morphologically similar, plate 29 being centered at $l = 140°$, $b = -14°$, below the Galactic plane and toward the anticenter, and plate 65 being centered at $l = 56°$, $b = 23°$, well above the Galactic plane. The third region contains clouds 54 and 55 of Magnani, Blitz, and Mundy (1985, hereafter MBM). The center of this region is located approximately at $l = 90°$, $b = -40°$. It appears distinctly different from the other two plates, consisting of an elongated structure containing internal structures that are similarly oriented. Plate 29 and MBM 54–55 are shown as contour/gray-scale plots in Figures 1*a* and 1*b*, respectively.

The region containing MBM clouds 54 and 55 was chosen because it was known to contain CO. Plates 29 and 65 were chosen because of their visual appearance in the infrared. It was not known whether CO-containing clouds were present in those regions.

III. CORRELATION RESULTS

Once the zodiacal emission was removed, we proceeded with the main task of calculating the fractal dimension of the clouds. When we slice an image at a certain contour level, we produce a set of objects which we will call clouds. We define the boundary of a cloud by this brightness contour level. Thus, we take each set of connected pixels above a given brightness level as a

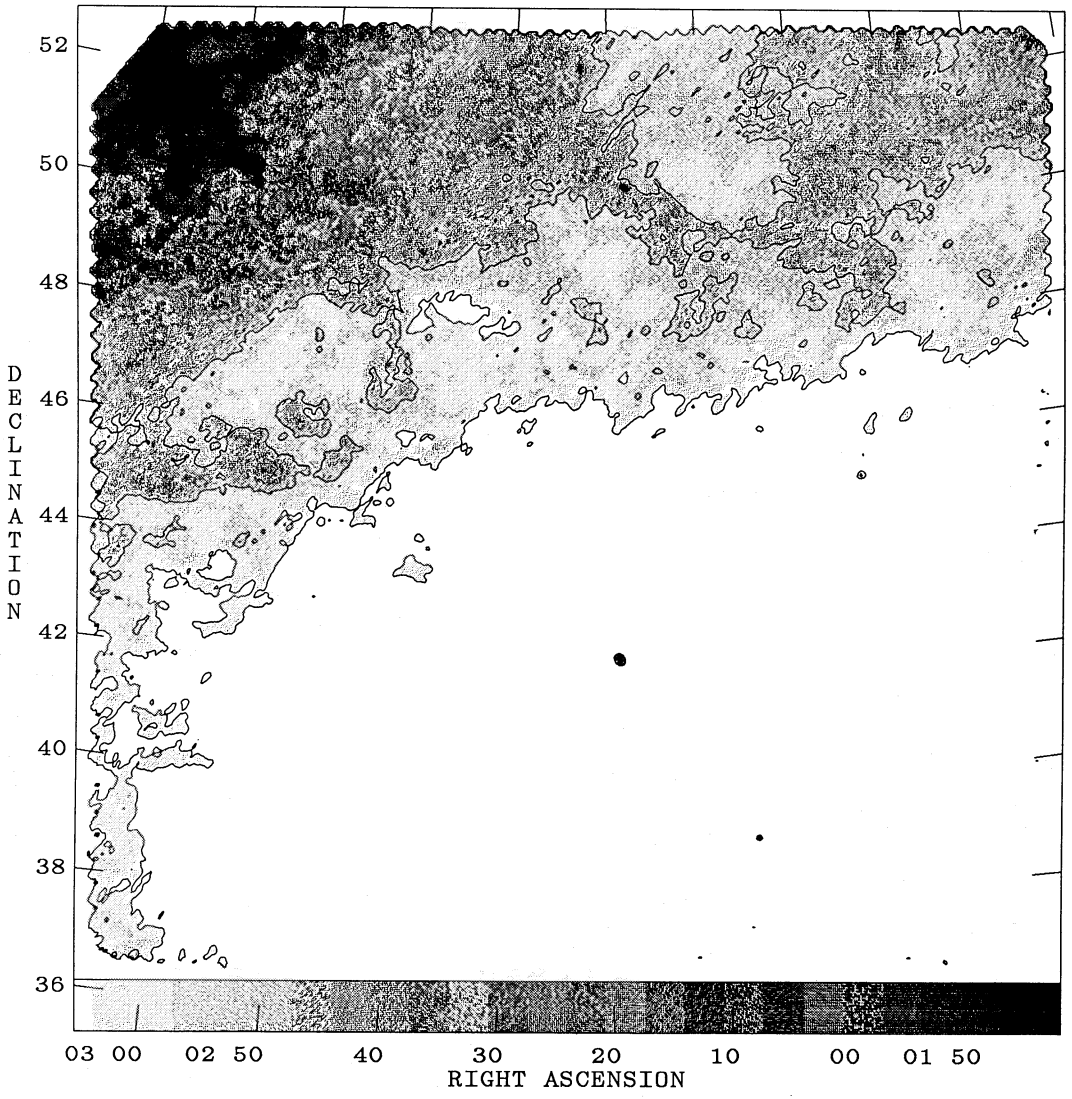

FIG. 1*a*

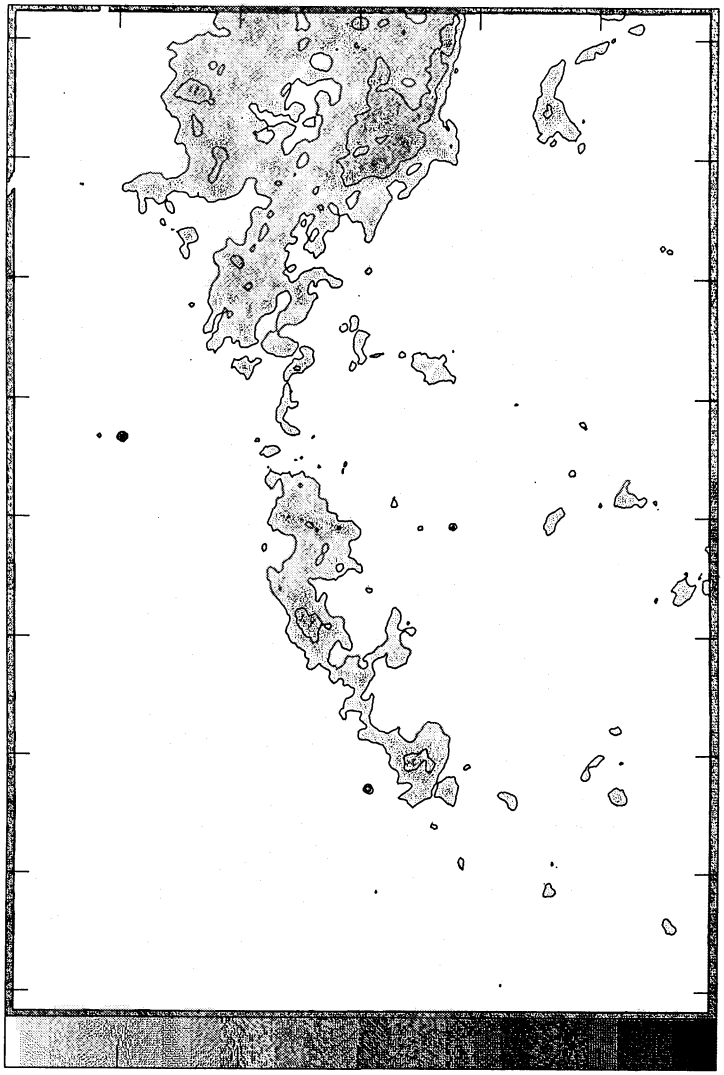

FIG. 1*b*

FIG. 1.—Shown are 100 μm contour/gray-scale plots of plate 29 and MBM 54–55. The contours are at 4 and 7 MJy sr^{-1} and define cloud used in the calculations. Images are linearly gray-scaled between the same limits. If a cloud intersects the edge of the image, it is not used in the calculations. Note that the very irregular structure of the cloud perimeters is apparent on all scales. (*a*) *IRAS* Sky Flux Plate 29. (*b*) MBM clouds 54 and 55; center of the image is at approximately R.A. 23^{h}04^m, decl. + 16°.

separate cloud. Pixels are said to be connected if they have a side in common, but not if they touch only at a corner.

The area of each cloud was found by counting the number of pixels contained within the threshold region. Each pixel within the cloud boundary contributes one unit (2′ × 2′ square) to the area.

In order to find the perimeter of a cloud, two different methods of calculation were used. The first method involved simply counting the number of noncloud pixels bordering a cloud pixel. This method will give the exact perimeter for rectangular objects, while it tends to underestimate the perimeter of circles by a few percent for radii above about 8 pixels.

The second method used was based upon Crofton's theorem (Santalo 1976) which states that half the integral over all angles of the projected entering width of an object equals the object's perimeter. (For example, the projected entering width of a circle of radius r is $2r$, since it looks like a line when viewed from the edge. For an annulus of outer radius r and inner radius a the projected entering width is $2r + 2a$, since a ray would enter the object twice if it passed within a radius a of the center.) The integral was evaluated from eight different angles. This method tends to overestimate the perimeter of circles. The fractional error in each method is, however, essentially constant, and this translates into an offset in the log-log plot of perimeter versus area. We find that the two methods give slopes and intercepts that differ by about 1% and 10% respectively. Our results are based upon the first method of calculating the perimeter.

For small objects, those comprising only a few pixels, one would expect large fractional errors in the calculation of both the area and the perimeter. Furthermore, we made no attempt to remove point source or compact source contamination for our images. Any such emission would show up as data points with small area and perimeter. For these reasons we did not include in the fit clouds that had an area less than a threshold of 13 pixels. The reason for this choice of threshold area and its effect on our results is discussed in more detail below.

At each brightnesss level we find that the largest clouds may not be completely contained within the Sky Flux plate. Furthermore, in some cases some of the smaller clouds may border the edge of the plate. In order to avoid biasing our results, we excluded from our data clouds that were not completely contained within the image.

We performed an unweighted linear least-squares fit to the data above the threshold of 13 pixels in area, where log area was the abscissa and log perimeter was the ordinate. A representative plot of the data is shown in Figure 2, and a summary of our results is presented in Table 1. The dimension quoted in the table for each contour level is twice the slope of the correlation plot, and the average values are weighted by the inverse square of the standard error. Also given are the number of clouds, the intercept, and the correlation coefficient at each contour level.

All three images range in brightness from about 1 MJy sr^{-1} to 12 MJy sr^{-1} typical of cirrus clouds. The contour levels we used were chosen to span this range while also producing clouds that spanned a reasonable range of sizes. In particular, high contour levels clip the peaks of the image and produce clouds that are small, leaving only a small range of sizes to fit.

It is apparent that the linear correlation for each ensemble of clouds is very good over more than two decades in area. The quoted average values of dimension and offset are the weighted

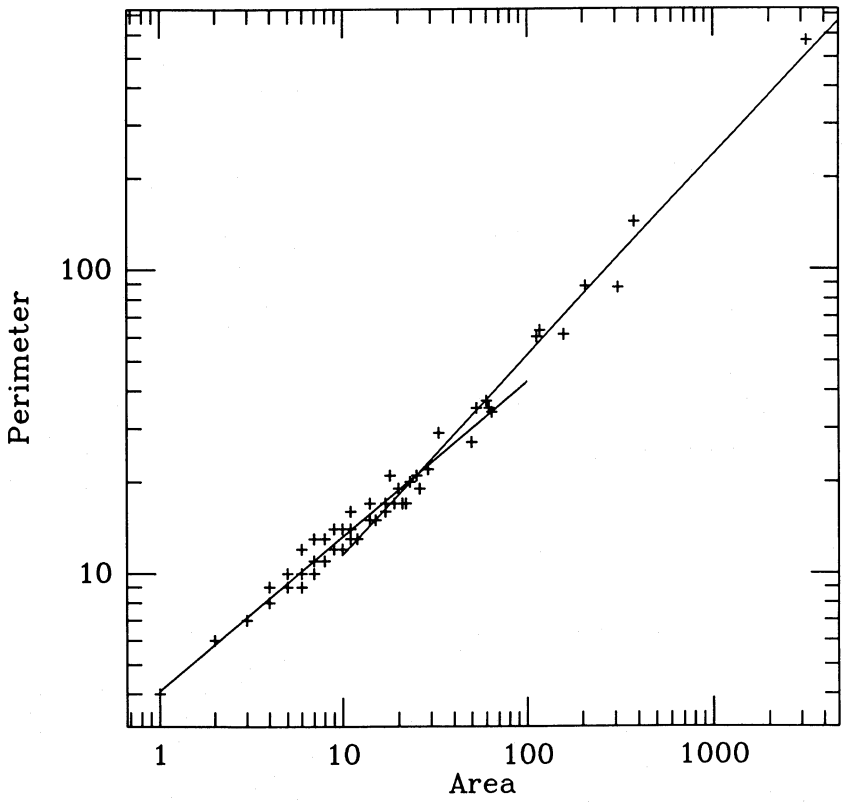

FIG. 2.—Area-perimeter plot of clouds from plate 65 defined by a 5 MJy sr^{-1} brightness contour. Units are pixels as described in the text. The two lines represent the best linear fits to the data above and below a threshold in area of 13 pixels. The slope of the upper line is 0.655 = $D/2$.

TABLE 1

BEST-FIT PARAMETERS FOR CLOUDS ABOVE A THRESHOLD AREA OF 13 PIXELS

Contour (MJy sr^{-1})	Number of Clouds	Dimension	Intercept	Correlation Coefficient
Plate 65:				
2	49	1.40 ± 0.038	0.382 ± 0.031	0.9824
3	37	1.27 ± 0.040	0.474 ± 0.034	0.9822
5	42	1.31 ± 0.026	0.402 ± 0.024	0.9926
7	32	1.19 ± 0.056	0.484 ± 0.042	0.9686
8	44	1.22 ± 0.028	0.429 ± 0.026	0.9900
Average	...	1.28 ± 0.04	0.424 ± 0.031	...
Plate 29:				
2	45	1.32 ± 0.036	0.412 ± 0.031	0.9834
3	38	1.24 ± 0.040	0.454 ± 0.032	0.9821
5	28	1.28 ± 0.017	0.414 ± 0.016	0.9978
7	55	1.26 ± 0.030	0.437 ± 0.026	0.9853
8	60	1.21 ± 0.026	0.461 ± 0.024	0.9869
Average	...	1.26 ± 0.03	0.431 ± 0.026	...
MBM 54–55:				
2	37	1.37 ± 0.052	0.380 ± 0.040	0.9752
3	57	1.28 ± 0.028	0.420 ± 0.024	0.9871
5	34	1.23 ± 0.033	0.448 ± 0.028	0.9884
7	15	1.33 ± 0.049	0.366 ± 0.044	0.9911
8	19	1.12 ± 0.038	0.520 ± 0.032	0.9987
Average	...	1.25 ± 0.04	0.436 ± 0.034	...

averages across the several contour levels for which the calculation was performed, where the weights are given by the inverse squares of the standard errors. There is clearly variation of D for a given ensemble of clouds as a function of contour level, and perhaps there is also a trend toward lower dimension at higher contour level as seen in Figure 3. The 2 MJy sr^{-1} contour level may be slightly corrupted by the stripiness of the images, increasing the calculated dimension. If this level is eliminated from the plot, the trend becomes less obvious. We found that the striping is not especially apparent for higher contour levels.

The results presented in Table 1 show that the dimensions and offsets for all three regions are quite close in value. While similar characteristics might be expected for plates 29 and 65 because of their similar morphologies, it is interesting that the dimension and offset of MBM 54–55 correspond closely to those of the other two images despite its apparent different structure.

In order to investigate the effect of the small clouds on the slope of the log P–log A diagram, we have plotted the slope as a function of threshold area as shown in Figure 4. For each of the three images we found the dimension of the perimeter for each of five contour levels. For 10 of the resulting perimeter-area diagrams the slope remains constant above a threshold area of 13 pixels, with the variation in the slope remaining within the error bars down to a threshold of 8 or 10 pixels. In the other five cases, the slope continues to increase as the threshold is pushed up. This is in part because of the sparsity and scatter of the data at large values of area, and we cannot conclude that there is a statistically significant trend of increasing slope as a function of threshold. In Table 1 we have reported the slope calculated at a threshold of 13 pixels, i.e., only including clouds with an area above 13 pixels.

IV. DISCUSSION

The procuedure outlined above allows us to establish the self-similarity and therefore the fractal dimension of a given cloud or cloud complex at a specific brightness level. The value we find for D is 1.26 ± 0.04, which is significantly different from 1, the value for a simple smooth curve. Furthermore, we find that the fractal dimension is characteristic of all brightness levels and remains constant from region to region even if the regions are morphologically different. While our sample of clouds was limited by the size of the Sky Flux plates (approximately 16° × 16°), and, more important, because we discarded clouds with area less than about 13 pixels, we see no evidence that the slope varies systematically outside the range we have studied. Hence, the correlation may well extend to larger and smaller cloud sizes.

It is important to understand the physical meaning of the dimension we have derived. The dimension of an object is a measure of how it fills space. For example, the dimension of the perimeter of a cloud is greater than unity because the curve representing the perimeter is convoluted like a coastline and not a simple curve like a circle. Furthermore, this convoluted behavior exists over a range of scale sizes that determines the limits of validity of the fractal characterization. The fact that the dimension is a constant, i.e., does not depend on the size of the object, is a statement of the scale invariance of the curve when viewed at differing resolutions.

The frequent assumption of spherical symmetry of a cloud also tacitly includes the assumption that the cloud completely fills space. These are two different properties which relate respectively to the intercept and the slope of our area-perimeter plots. The intercept is characteristic of the shape of the object, being different for a circle or an ellipse, for example, both of which have the same dimension. The fact that we find a constant value for the intercept implies that the characteristic shapes of all the clouds studied are essentially the same.

There are a number of consequences of having a non–space-filling cloud. Because the dimension characterizes how much material is contained within a given radius, the mass of material in a fractal cloud will be less than expected for a similar space-filling cloud.

One should also be careful not to misinterpret the meaning of the fractal dimension we have calculated. This dimension

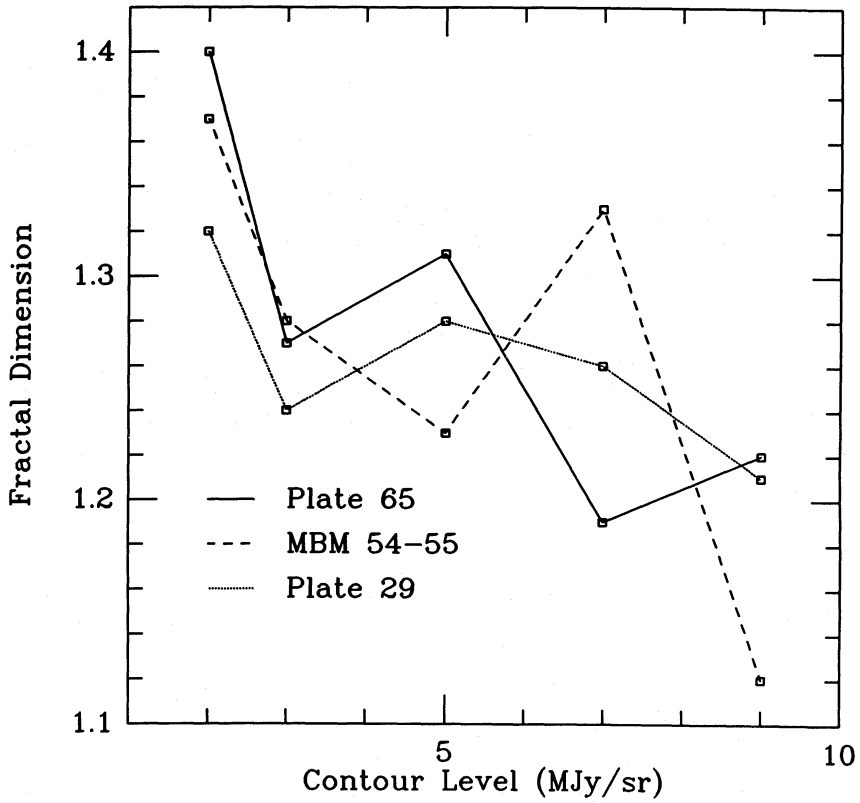

FIG. 3.—Plot of fractal dimension as a function of contour level. There is an apparent trend toward lower dimension at higher contour level. This is less obvious if the 2 MJy sr^{-1} data points are eliminated. See text for more details.

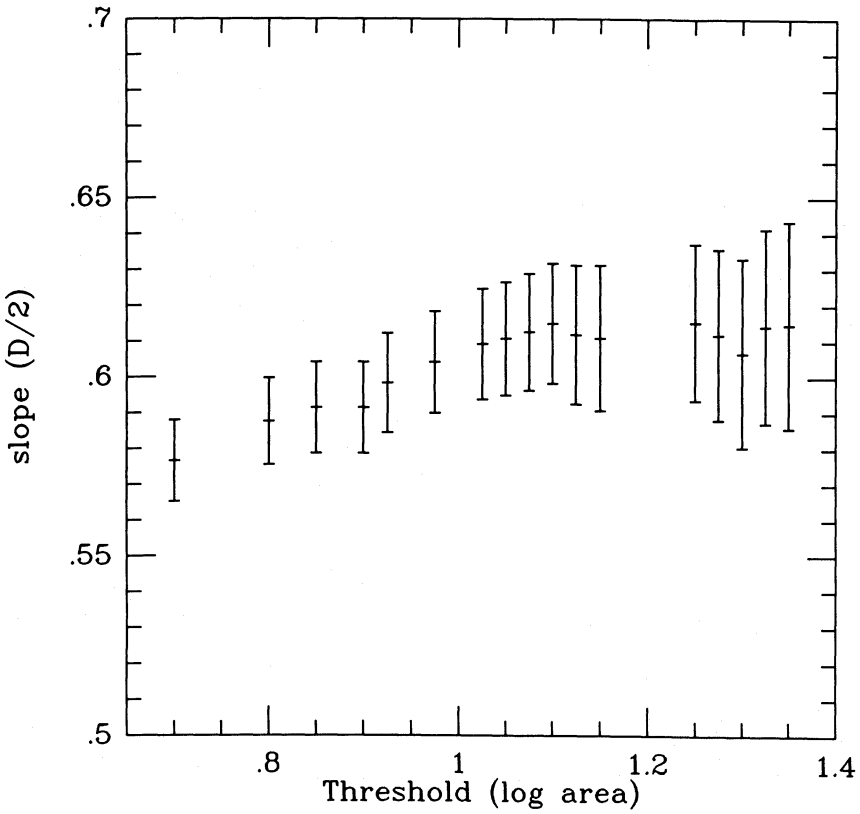

FIG. 4.—Slope of log area–log perimeter plot as a function of threshold for data above the threshold. Data correspond to clouds defined by the 5 MJy sr^{-1} contour level for MBM clouds 54 and 55. Slope shows no trend above a threshold of about 13 pixels (1.1 in logarithm).

refers to the scaling properties of the perimeter of a cloud. The size distribution of clouds may also follow a power law whose exponent can be interpreted as a fractal dimension. Thus, a collection of clouds can be characterized by a number of fractal dimensions each referring to different geometrical properties, and the physical basis of each has to be understood.

Because it is useful to view the interstellar medium as a turbulent fluid for purposes of modeling (Scalo 1987), we can try to interpret the fractal dimension of clouds in terms of a simple turbulence model. A number of authors have investigated the relationship between fractals and turbulence; see, for example, Hentschel and Procaccia (1984) and Mandelbrot (1975).

Following Hentschel and Procaccia (1984), we can view the dimension of the cloud as the dimension of a surface on which turbulent activity is concentrated. This means that one has an increased probability of finding material in certain active regions. Thus, rather than having a uniform space-filling cloud, one finds material concentrated on a surface of dimension less than 3. This fractal surface is characteristic of the three-dimensional structure of the cloud and therefore allows us to make a connection between the observations and the scaling properties of physical quantities of interest.

All of the clouds we have examined are cirrus which are known to be optically thin in the infrared and generally have an optical depth in the visible of order 0.5 or 1 (Low *et al.* 1984; Weiland *et al.* 1986). We therefore take our clouds to be defined by contours of constant column density.

If the mass within a volume of radius r scales as $m \sim r^{D'}$ and the volume scales as $V(r) \sim r^3$, we can infer that the density of emitting material must scale as

$$\rho \sim r^{D'-3} . \tag{3}$$

Our observations tell us how the mass column density, as measured by infrared brightness, scales as a function of projected radius s. One would like to relate the observed dimension D' to the true dimension D. It is not immediately obvious how to make this connection. It has been shown (Hentschel and Procaccia 1984; Rys and Waldvogel (1986) that if one takes a two-dimensional slice through a fractal of dimension $D \geq 2$, the dimension of the resulting curve is $D - 1$. Our observations, however, correspond to a cloud (a three-dimensional fractal structure) projected onto a two-dimensional surface, so this relationship would not necessarily apply. In order to test equation (3), one would have to make measurements of density as a function of volume for a single cloud.

A separate projection effect is also possible. If a field of view contains numerous distinct clouds whose size distribution follows a power law and the clouds overlap along the line of sight, the apparent structure (again defined by contours of constant column density) can have a fractal dimension different from (in general larger than) the dimension of the small clouds. This effect has been seen in simulations using spherical clouds by Houlahan and Scalo (1987). It is difficult to determine whether or not this is an important effect for our clouds, since we have no way to determine their three-dimensional structure. For gas clouds such as CO where there is velocity information, one could hope to determine the three-dimsensional structure and see whether projection effects are important.

We gratefully acknowledge the very helpful comments provided by E. Dwek, R. Isaacman, D. Leisawitz on early drafts of this work. We also thank the referee, John Scalo, for his insightful comments. This research was performed in the Laboratory for Astronomy and Solar Physics at Goddard Space Flight Center under National Aeronautics and Space Administration contract 77/NAS5-28771: Scientific Support for the Cosmic Background Explorer while one of us (F. X. D.) held a National Research Council Associateship. This paper was taken from a dissertation to be submitted to the Graduate School, University of Maryland, by David Bazell in partial fulfillment of the requirements for the Ph.D. degree in physics.

REFERENCES

Henderson-Sellers, A. 1986, *Quart. J.R.A.S.*, **27**, 90.
Hentschel, H. G. E., and Procaccia, I. 1984, *Phys. Rev. A*, **29**, 1461.
Houlahan, P., and Scalo, J. 1987, private communication.
Lovejoy, S. 1982, *Science*, **216**, 185.
Low, F. J., *et al.* 1984, *Ap. J. (Letters)*, **278**, L19.
Magnani, L., Blitz, L., and Mundy, L. 1985, *Ap. J.*, **295**, 402.
Mandelbrot, B. B. 1975, *J. Fluid Mech.*, **72**, 401.
———. 1983, *The Fractal Geometry of Nature*, (New York: Freeman).
Rys, F. S., and Waldvogel, A. 1986, *Phys. Rev. Letters*, **56**, 784.
Santalo, L. A. 1976, *Integral Geometry and Geometric Probability* (Reading: Addison-Wesley).
Scalo, J. M. 1987, in *Interstellar Processes*, ed. D. J. Hollenbach and H. A. Thronson, Jr. (Dordrecht: Reidel).
Verter, F. 1987, *Techniques for Removing Zodiacal Emission from IRAS Sky Flux Plates* (NASA Rept., Laboratory for Extraterrestrial Physics).
Weiland, J. L., Blitz, L., Dwek, E., Hauser, M. G., Magnani, L., and Rickard, L. J. 1986, *Ap. J. (Letters)*, **306**, L101.

DAVID BAZELL: Applied Research Corporation, 8201 Corporate Drive, Landover, MD 20785

F. XAVIER DÉSERT: NASA, Code 685, Laboratory for Astronomy and Solar Physics, Goddard Space Flight Center, Greenbelt, MD 20771